arXiv:1111.3826v1 [physics.optics] 16 Nov 2011

Linear and Nonlinear Pulse Propagations in Lifetime-Broadened Atomic Media with Spontaneously Generated Coherence

Chao Hang and Guoxiang Huang

State Key Laboratory of Precision Spectroscopy and Department of Physics, East China Normal University, Shanghai 200062, China

(Dated: November 17, 2011)

Abstract

The linear and nonlinear pulse propagations in lifetime-broadened three-state media with spontaneously generated coherence (SGC) are investigated theoretically. Three generic systems of V-, Λ-, and Ξ-type level configurations are considered and compared. It is shown that in linear propagation regime the SGC in the V-type system can result in a significant change of dispersion and absorption and may be used to completely eliminate the absorption and largely reduce the group velocity of a probe field. However, the SGC has no effect on the dispersion and absorption of the Λ- and Ξ-type systems. In nonlinear propagation regime, the SGC displays different influences on Kerr nonlinearity for different systems. Specifically, it can enhance the Kerr nonlinearity of the V-type system whereas weaken the Kerr nonlinearity of the Λ-type system. Using the SGC, stable optical solitons with ultraslow propagating velocity and very low pump power can be produced in the V-type system by exploiting only one laser field in the system.

PACS numbers: 42.65.Tg, 05.45.Yv

I. INTRODUCTION

The propagation of linear and nonlinear light pulses in coherent atomic media has been an important subject of many recent studies, such as formation of simultons and adiabatons [1], group-velocity reduction [2], storage and retrieval of light [3, 4], and single-photon pulse propagation [5]. Among various coherent preparation techniques studied so far, electromagnetic induced transparency (EIT) is perhaps the most extensively investigated one because of its diverse practical applications [6]. Due to the quantum interference induced by a coupling laser field, a probe laser field propagating in an EIT medium can avoid a large absorption even when it is tuned to a strong one-photon resonance. EIT media also exhibit drastic change of dispersion and giant enhancement of Kerr nonlinearity, resulting in various nonlinear optical phenomena such as high-efficient frequency conversions [7, 8], temporal and spatial optical solitons at very low light level [9–12]. As a powerful technique, EIT has been used to study the property of Rydberg atomic ensembles very recently [13].

In an EIT medium, it is crucial to have at least two laser fields as they are necessary to be used to create atomic coherence. Besides the EIT technique, an atomic coherence can also be created by the quantum interference between two spontaneous emission channels without using any coupling laser field, which is called the spontaneously generated coherence (SGC). In recent years, much attention has been paid to the study on SGC and related topics, including lasing without inversion [14–16], coherent population trapping [17], spectral narrowing and fluorescence quenching [18–21], fluorescence squeezing [22], giant self-phase modulation [23], ground-state quantum beats [24], cavity-mode entanglement [25], electromagnetically induced grating [26], and so on.

Although a large amount of research activities have been made on SGC, most of them are, however, focused on the static property of various systems, and only a few works dedicate to the study of pulse propagation in SGC media. Here we mention the work by Paspalakis *et al.* [27] who studied the pulse propagation in a four-level system, where a ground state is coupled to two closely spaced excited states by a laser field with both excited states decaying into a common continuum. Strong, short laser pulses with adiabaton-like property were observed by using numerical simulations.

In this article, we investigate, both analytical and numerically, the linear and nonlinear pulse propagations in lifetime-broadened three-state media with SGC. In stead of adiabatons,

we consider breather-like nonlinear excitations without using any adiabatic approximation. Our work includes two aspects: (i) We consider three generic systems of V-, Λ-, and Ξ-type level configurations, and compare their linear propagating property with the SGC effect being taken into account. We show that the SGC in the V-type system can result in a significant change of dispersion and absorption and may be used to completely eliminate the absorption and largely reduce the group velocity of probe field. However, the SGC has no effect on the dispersion and absorption of the Λ- and Ξ-type systems. (ii) We demonstrate that in nonlinear propagation regime, the SGC has different influences on Kerr nonlinearity for different systems. In particular, it can enhance the Kerr nonlinearity of the V-type system but weaken the Kerr nonlinearity of the Λ-type system. By using the SGC, stable optical solitons with ultraslow propagating velocity and very low pump power can be produced in the V-type system. We stress that the scheme for generating ultraslow optical solitons presented here is very different from those in Refs. [9–12] because the suppression of optical absorption and the reduction of group velocity are not contributed by an additional control field but by the SGC and hence only a single laser field is needed.

The work reported here is arranged as follows. In Sec. II, three-level models of V-, Λ-, and Ξ-type configurations with SGC are introduced. Linear pulse propagations are discussed and dispersion and absorption properties for three different systems are analyzed. In Sec. III, the Kerr nonlinearity of the V- and Λ-type systems are analyzed, and ultraslow optical solitons at very low light level are obtained. In Sec. IV, a discussion of open system is made. The last section contains a summary of our main results.

II. MODELS AND PULSE PROPAGATION IN LINEAR REGIME

For comparison and also for completeness, we investigate three generic three-state systems of V-, Λ-, and Ξ-type level configurations, which are considered separately in the following.

A. V-type system

We first consider a three-level V-type atomic system, as shown in Fig. 1(a), in which two closely spaced excited states $|2\rangle$ and $|3\rangle$ decay simultaneously into the ground state $|1\rangle$ by the spontaneous emission with decay rates Γ_2 and Γ_3, respectively. The quantum

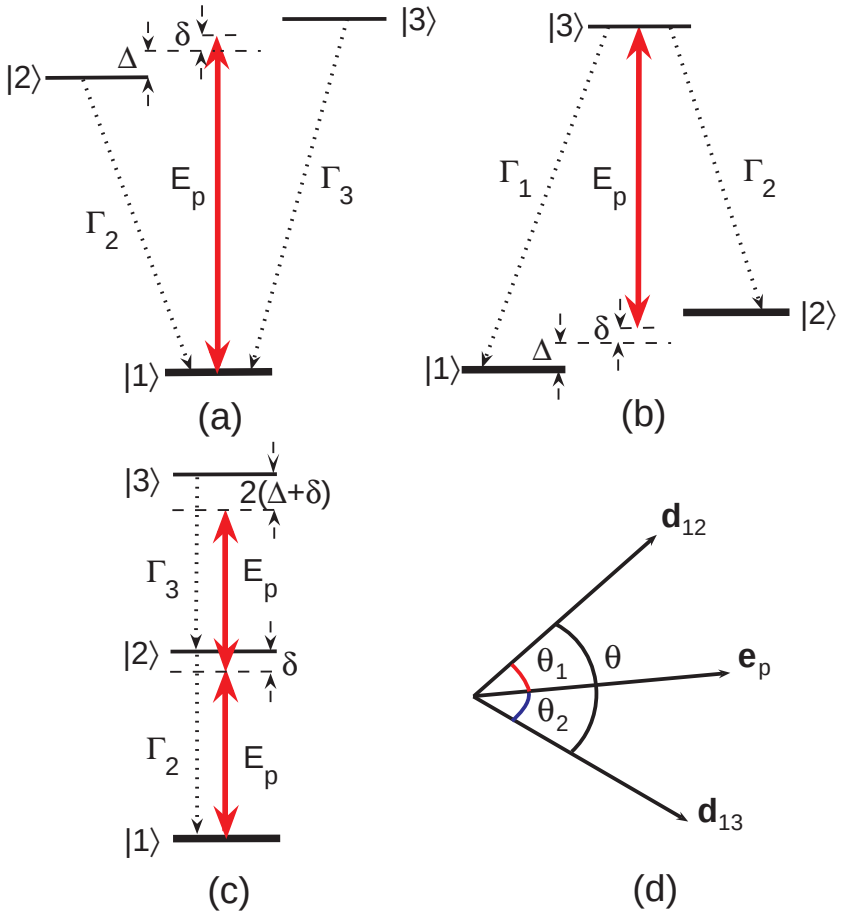

FIG. 1: (color online) Energy level diagrams and excitation schemes of lifetime-broadened three-level systems with SGC. (a): V-type system; (b): Λ-type system; (c): Ξ-type system. $|j\rangle$ ($j = 1, 2, 3$) are atomic bare states, $\mathbf{E}_p$ is weak probe laser field, Δ and δ are detunings, and Γ_j ($j = 1, 2$) are decay rates of relevant states. (d): The definition of the alignment angles (θ_1, θ_2) of the dipole matrix elements ($\mathbf{d}_{12}$, $\mathbf{d}_{13}$) related to the unit polarization vector $\mathbf{e}_p$ of the probe field. $\theta = \theta_1 + \theta_2$ is the angle between $\mathbf{d}_{12}$ and $\mathbf{d}_{13}$.

interference between the two decay channels (from $|2\rangle$ to $|1\rangle$ and $|3\rangle$ to $|1\rangle$) results in the SGC of the system [28]. A weak, pulsed probe field (with duration τ_0) of center frequency ω_p and wavevector $\mathbf{k}_p$, i.e.,

$$\mathbf{E}_p(\mathbf{r}, t) = \mathbf{e}_p \mathcal{E}_p(\mathbf{r}, t) e^{i(\mathbf{k}_p \cdot \mathbf{r} - \omega_p t)} + \text{c.c}, \tag{1}$$

couples the ground state $|1\rangle$ to the excited states $|2\rangle$ and $|3\rangle$, where $\mathbf{e}_p$ and $\mathcal{E}_p(\mathbf{r}, t)$ are the unit polarization vector and envelope function of the probe field, respectively.

Under electric-dipole, rotating-wave, and Weisskopf-Wigner approximations, the equa-

tions of motion for the density matrix governing atomic dynamics are

$$\dot{\rho}_{22} = -\Gamma_2\rho_{22} + i\Omega_p\rho_{12} - i\Omega_p^*\rho_{21} - \eta\frac{\sqrt{\Gamma_2\Gamma_3}}{2}(\rho_{23}+\rho_{32}), \tag{2a}$$

$$\dot{\rho}_{33} = -\Gamma_3\rho_{33} + ip\Omega_p\rho_{13} - ip\Omega_p^*\rho_{31} - \eta\frac{\sqrt{\Gamma_2\Gamma_3}}{2}(\rho_{23}+\rho_{32}), \tag{2b}$$

$$\dot{\rho}_{21} = \left[i\left(\Delta+\delta\right) - \frac{\Gamma_2}{2}\right]\rho_{21} + i\Omega_p(\rho_{11}-\rho_{22}) - ip\Omega_p\rho_{23} - \eta\frac{\sqrt{\Gamma_2\Gamma_3}}{2}\rho_{31}, \tag{2c}$$

$$\dot{\rho}_{31} = \left[i\left(-\Delta+\delta\right) - \frac{\Gamma_3}{2}\right]\rho_{31} + ip\Omega_p(\rho_{11}-\rho_{33}) - i\Omega_p\rho_{32} - \eta\frac{\sqrt{\Gamma_2\Gamma_3}}{2}\rho_{21}, \tag{2d}$$

$$\dot{\rho}_{32} = -\left(i2\Delta + \frac{\Gamma_2+\Gamma_3}{2}\right)\rho_{32} - i\Omega_p^*\rho_{31} + ip\Omega_p\rho_{12} - \eta\frac{\sqrt{\Gamma_2\Gamma_3}}{2}(\rho_{22}+\rho_{33}), \tag{2e}$$

with $\rho_{11}+\rho_{22}+\rho_{33}=1$. Here $\Omega_p = \mathbf{e}_p\cdot\mathbf{d}_{12}\mathcal{E}_p/\hbar$ is half Rabi frequency of the probe field with $\mathbf{d}_{ij}\equiv\langle i|\mathbf{d}|j\rangle$ being the density-matrix elements related to states $|i\rangle$ and $|j\rangle$, $\Delta = (E_3-E_2)/(2\hbar)$ is half frequency difference between $|2\rangle$ and $|3\rangle$, and $\delta=\omega_p-(E_3+E_2)/(2\hbar)$ is one-photon detuning [see Fig. 1(a)]. The cross coupling term contributed by the SGC effect is manifested by the factor $\eta\sqrt{\Gamma_2\Gamma_3}/2$, with $\eta=\mathbf{d}_{12}\cdot\mathbf{d}_{13}/|\mathbf{d}_{12}||\mathbf{d}_{13}|=\cos\theta$ denoting the alignment of two dipole matrix elements $\mathbf{d}_{12}$ and $\mathbf{d}_{13}$, where θ is the misalignment angle between $\mathbf{d}_{12}$ and $\mathbf{d}_{13}$. If $\mathbf{d}_{12}$ and $\mathbf{d}_{13}$ are parallel (i.e. $\theta=0$), one has $\eta=1$, the system exhibits maximum SGC; if $\mathbf{d}_{12}$ and $\mathbf{d}_{13}$ are perpendicular (i.e. $\theta=\pi/2$), one has $\eta=0$, the system displays no SGC. $p=|\mathbf{e}_p\cdot\mathbf{d}_{13}|/|\mathbf{e}_p\cdot\mathbf{d}_{12}|=|\mathbf{d}_{13}|\cos\theta_1/[|\mathbf{d}_{12}|\cos\theta_2]$, where θ_1 (θ_2) is the misalignment angle between $\mathbf{d}_{12}$ ($\mathbf{d}_{13}$) and $\mathbf{e}_p$. In the following, we assume $|\mathbf{d}_{13}|\simeq|\mathbf{d}_{12}|$ and a particular case can be found that θ is equally partitioned by $\mathbf{e}_p$, i.e. $\theta_1\simeq\theta_2=\theta/2$, as did by Wan et al. [26]. In such case, we have $p\simeq1$ and η is still kept a free parameter with its value taking between -1 and 1 [see Fig. 1(d)].

The equation of motion for the probe-field Rabi frequency Ω_p can be obtained by using Maxwell equation. Under slowly-varying envelope approximation, it reads

$$i\left(\frac{\partial}{\partial z}+\frac{1}{c}\frac{\partial}{\partial t}\right)\Omega_p + \kappa(\rho_{21}+p\rho_{31}) = 0, \tag{3}$$

where $\kappa=\mathcal{N}_a\omega_p|\mathbf{e}_p\cdot\mathbf{d}_{12}|^2/(2\epsilon_0c\hbar)$ with $\mathcal{N}_a$ being the atomic concentration. For simplicity, we assume in the following that $\Gamma_2\approx\Gamma_3\equiv\Gamma$.

The linear optical response of the system can be obtained by solving the Maxwell-Bloch (MB) Eqs. (2) and (3). Assuming Ω_p is a small quantity, $\rho_{11}\approx1$, and ρ_{21}, ρ_{31}, and Ω_p are proportional to $\exp[i(Kz-\omega t)]$, we obtain the linear dispersion relation

$$K(\omega) = \frac{\omega}{c} - \kappa\left[\frac{\omega+d_3-ip\eta\Gamma/2}{D(\omega)} + \frac{p^2(\omega+d_2)-ip\eta\Gamma/2}{D(\omega)}\right], \tag{4}$$

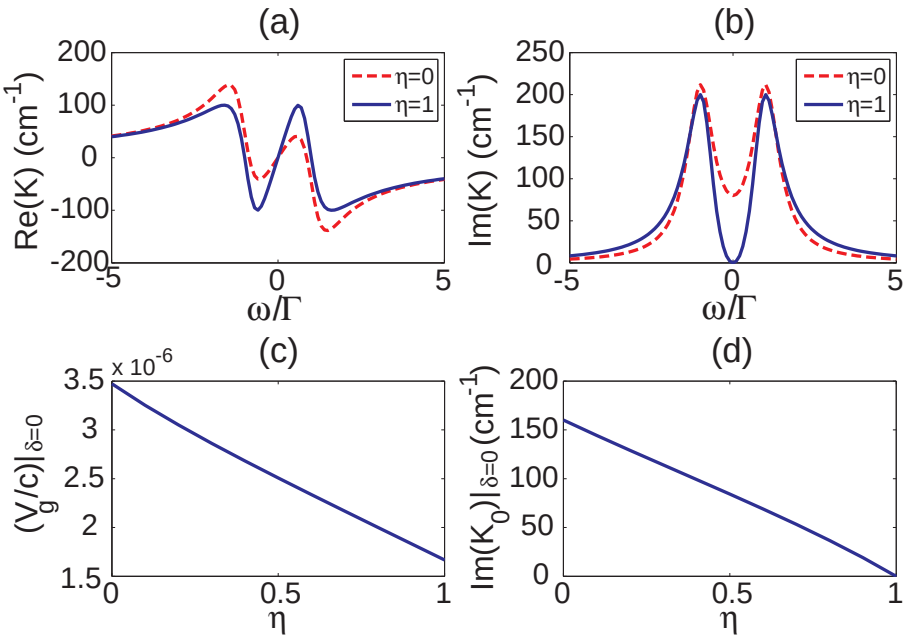

FIG. 2: (color online) (a), (b): Re(K) and Im(K) as functions of ω/Γ with maximum SGC (i.e. $\eta = 1$; the solid line) and without SGC (i.e. $\eta = 0$; the dashed line). (c), (d): $\mathrm{Im}(K_0)|_{\delta=0}$ and $(V_g/c)|_{\delta=0}$ as functions of η.

where $D(\omega) = (\omega + d_2)(\omega + d_3) + \eta^2\Gamma^2/4$ with $d_2 = \Delta + \delta + i\Gamma/2$, and $d_3 = -\Delta + \delta + i\Gamma/2$. By Taylor expanding $K(\omega)$ around $\omega = 0$ [29], we obtain $K(\omega) = K_0 + K_1\omega + \frac{1}{2}K_2\omega^2 + \cdots$, with the expansion coefficients $K_j = [\partial^j K(\omega)/\partial\omega^j]|_{\omega=0}$ ($j = 0,\ 1,\ 2, \cdots$) explicitly given by

$$K_0 = -\kappa\frac{p^2 d_2 + d_3 - ip\eta\Gamma}{d_2 d_3 + \eta^2\Gamma^2/4}, \tag{5a}$$

$$K_1 = \frac{1}{c} - \kappa\frac{1+p^2}{d_2 d_3 + \eta^2\Gamma^2/4} + \kappa\frac{(p^2 d_2 + d_3 - ip\eta\Gamma)(d_2 + d_3)}{(d_2 d_3 + \eta^2\Gamma^2/4)^2}, \tag{5b}$$

$$K_2 = 2\kappa\frac{(1+p^2)(d_2+d_3)}{(d_2 d_3 + \eta^2\Gamma^2/4)^2} + 2\kappa\frac{p^2 d_2 + d_3 - ip\eta\Gamma}{(d_2 d_3 + \eta^2\Gamma^2/4)^2} - 2\kappa\frac{(p^2 d_2 + d_3 - ip\eta\Gamma)(d_2+d_3)^2}{(d_2 d_3 + \eta^2\Gamma^2/4)^3} \tag{5c}$$

Here, $K_0 = \mathrm{Re}(K_0) + i\mathrm{Im}(K_0)$ gives the phase shift per unit length and absorption coefficient, K_1 determines the group velocity V_g ($\equiv 1/K_1$), and K_2 represents the group-velocity dispersion.

Shown in Shown in Fig. 2(a) and Fig. 2(b) are respectively the real part and imaginary part of K as functions of ω, which characterize the dispersion and absorption of the system. The solid lines in the figure are for the case with the maximum SGC (i.e. $\eta = 1$), whereas the dashed lines are for the case without the SGC (i.e. $\eta = 0$). System parameters are chosen as $\kappa = 1.0 \times 10^9$ cm^{-1}s^{-1}, $\Gamma = 1.0 \times 10^7$ s^{-1}, $\Delta = 1.0 \times 10^7$ s^{-1}, $\delta = 0$, and $p = 1$. We

see that in the region around $\omega = 0$ the probe-field displays a drastic change of dispersion (and hence a drastic reduction of group velocity) (panel (a)) and a large suppression of absorption (panel (b)). Obviously, the reduction of group-velocity and the suppression of absorption with the SGC are much more significant than those without the SGC. These can be seen also by the expression of the group velocity and the absorption coefficient at $\delta = 0$:

$$V_g|_{\delta=0} = \left\{ \frac{1}{c} + 2\kappa \frac{\Delta^2 - (1-\eta)^2\Gamma^2/4}{[\Delta^2 + (1-\eta^2)\Gamma^2/4]^2} \right\}^{-1}, \tag{6a}$$

$$\mathrm{Im}(K_0)|_{\delta=0} = \frac{\kappa(1-\eta)\Gamma}{\Delta^2 + (1-\eta^2)\Gamma^2/4}, \tag{6b}$$

which are respectively shown in the panels (c) and (d) of Fig. 2. Notice that the group velocity of the probe field can be lowered by increasing the SGC effect (panel (c)). If $\eta = 1$ one has $\mathrm{Im}(K_0)|_{\delta=0} = 0$, i.e. the absorption of the probe field can be completely eliminated by means of the SGC. But if the SGC is absent (i.e. $\eta = 0$), $\mathrm{Im}(K_0)|_{\delta=0}$ is not only non-zero but also with a large positive value, and hence the probe-field absorption is quite significant (panel (d)). Consequently, in the absence of the SGC the probe filed can not propagate to a long distance.

It is instructive to discuss the SGC effect on the probe-field absorption in more details. From Fig. 2(b), we see that the probe-field absorption is suppressed around $\omega = 0$ in both cases with and without the SGC, resulting in the appearance of transparency windows in the absorption spectrum. However, the depth and width of the transparency windows are quite different. The transparency window with the SGC ($\eta = 1$; the solid line) is much more deeper and wider than that without the SGC ($\eta = 0$; the dashed line).

The difference for the absorption spectra for the above two cases can be understood more clearly as follows. For illustration, we split the imaginary part of K into the form

$$\begin{aligned} \mathrm{Im}(K) = \quad & \kappa \left[\frac{\Gamma}{2} \left(\frac{1}{(\omega+\delta-v)^2 + \Gamma^2/4} + \frac{1}{(\omega+\delta+v)^2 + \Gamma^2/4} \right) \right. \\ & \left. + \frac{\eta\Gamma}{2v} \left(\frac{\omega+\delta-v}{(\omega+\delta-v)^2 + \Gamma^2/4} - \frac{\omega+\delta+v}{(\omega+\delta+v)^2 + \Gamma^2/4} \right) \right], \end{aligned} \tag{7}$$

with $v = \sqrt{\Delta^2 - \eta^2\Gamma^2/4}$. The first two terms on the right hand side (RHS) of Eq. (7) correspond to two resonances of the excited states $|2\rangle$ and $|3\rangle$, shown by the dashed line of Fig. 3. The dip with a non-zero minimum in the dashed line can be interpreted as a gap between the two resonances, which is a typical character of Autler-Townes (AT) splitting [30]. The next two terms (interference terms) provide a gain (absorption) when $\eta > 0$

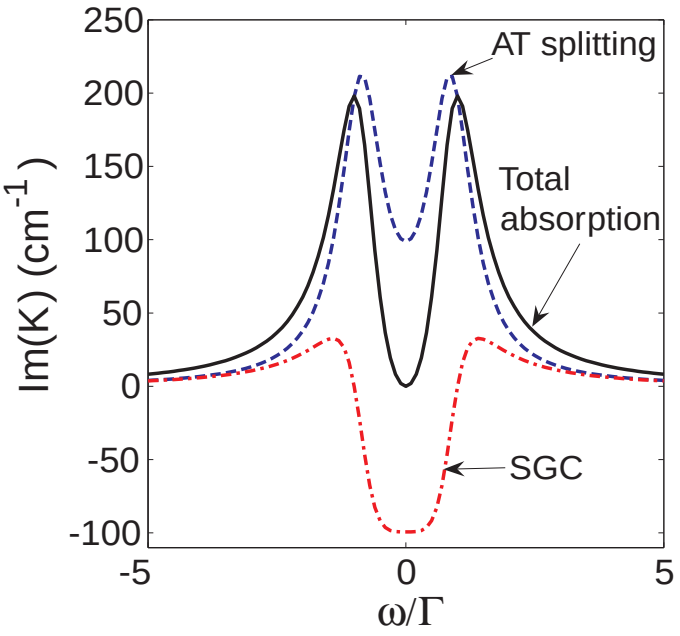

FIG. 3: (color online) The spectra of AT-splitting (dashed line), SGC (dotted line), and total absorption (solid line) as functions of ω/Γ with $\delta = 0$.

($\eta < 0$), shown in Fig. 3 by the dotted-dashed line. Such terms come from the quantum interference effect between two spontaneous emission channels (i.e. from $|2\rangle$ to $|1\rangle$ and from $|3\rangle$ to $|1\rangle$), a typical character of SGC. The sum of the four terms on the RHS of Eq. (7) is the total absorption of the probe field, shown by the solid line of Fig. 3. From these results we clearly see that it is the joint contribution from the AT splitting and the SGC effect that make the absorption of the probe field vanish, and hence providing the possibility for a long-distance transmission of the probe field in both the linear and nonlinear propagation regimes.

B. Λ-type system

We now consider a three-level Λ-type system, in which a weak probe field with the form (1) couples the excited state $|3\rangle$ to the two ground states $|1\rangle$ and $|2\rangle$, with corresponding spontaneous decay rates Γ_1 and Γ_2, respectively (see Fig. 1(b)). A SGC occurs by the quantum interference between two spontaneous decay channels from $|3\rangle$ to $|1\rangle$ and from $|3\rangle$ to $|2\rangle$ [31, 32].

The atomic dynamics of the system is described by the density matrix equations

$$\dot{\rho}_{11} = \Gamma_1\rho_{33} + ip\Omega_p^*\rho_{31} - ip\Omega_p\rho_{13}, \tag{8a}$$

$$\dot{\rho}_{22} = \Gamma_2\rho_{33} + i\Omega_p^*\rho_{32} - i\Omega_p\rho_{23}, \tag{8b}$$

$$\dot{\rho}_{21} = -i2\Delta\rho_{21} + i\Omega_p^*\rho_{31} - ip\Omega_p\rho_{23} + \eta\sqrt{\Gamma_1\Gamma_2}\rho_{33}, \tag{8c}$$

$$\dot{\rho}_{31} = \left[-i\left(\Delta+\delta\right) - \frac{\Gamma_1+\Gamma_2}{2}\right]\rho_{31} + ip\Omega_p(\rho_{11}-\rho_{33}) + i\Omega_p\rho_{21}, \tag{8d}$$

$$\dot{\rho}_{32} = \left[i(\Delta-\delta) - \frac{\Gamma_1+\Gamma_2}{2}\right]\rho_{32} + i\Omega_p(\rho_{22}-\rho_{33}) + ip\Omega_p\rho_{12}, \tag{8e}$$

with $\rho_{11}+\rho_{22}+\rho_{33}=1$. Here $\Omega_p = \mathbf{e}_p\cdot\mathbf{d}_{13}\mathcal{E}_p/\hbar$ is half Rabi frequency of the probe field, $\Delta = (E_2-E_1)/(2\hbar)$ is half frequency difference of two closely spaced ground-state levels, and $\delta = (2E_3-E_1-E_2)/(2\hbar)-\omega_p$ is one-photon detuning (see Fig. 1(b)). The SGC effect is still described by the factor $\eta\sqrt{\Gamma_1\Gamma_2}/2$, with $\eta = \mathbf{d}_{13}\cdot\mathbf{d}_{23}/|\mathbf{d}_{13}||\mathbf{d}_{23}|$.

The equation of motion for Ω_p is

$$i\left(\frac{\partial}{\partial z}+\frac{1}{c}\frac{\partial}{\partial t}\right)\Omega_p + \kappa(p\rho_{31}+\rho_{32}) = 0, \tag{9}$$

where $p = |\mathbf{e}_p\cdot\mathbf{d}_{13}|/|\mathbf{e}_p\cdot\mathbf{d}_{23}| = \cos\theta_1/\cos\theta_2$ ($|\mathbf{d}_{13}|\simeq|\mathbf{d}_{23}|$) and $\kappa = \mathcal{N}_a\omega_p|\mathbf{e}_p\cdot\mathbf{d}_{23}|^2/(2\epsilon_0 c\hbar)$. For simplicity, we assume in the following that $\Gamma_1\approx\Gamma_2=\Gamma$.

From the MB Eqs. (8) and (9) it is easy to obtain the linear dispersion relation of the system, which reads

$$K(\omega) = \frac{\omega}{c} - \kappa\left[p^2\frac{\rho_{11}^{(0)}}{\omega-d_1} + \frac{\rho_{22}^{(0)}}{\omega-d_2}\right], \tag{10}$$

where $d_1 = \Delta+\delta-i\Gamma$, $d_2 = -\Delta+\delta-i\Gamma$, $\rho_{11}^{(0)} = |d_1|^2/(|d_1|^2+p^2|d_2|^2)$, and $\rho_{22}^{(0)} = p^2|d_2|^2/(|d_1|^2+p^2|d_2|^2)$. As before, we Taylor expand $K(\omega)$ at $\omega=0$, i.e. $K(\omega) = K_0 + K_1\omega + \frac{1}{2}K_2\omega^2+\cdots$. The expansion coefficients $K_j = [\partial^j K(\omega)/\partial\omega^j]|_{\omega=0}$ ($j=0,\,1,\,2,\cdots$) are given by $K_0 = \kappa(p^2\rho_{11}^{(0)}/d_1+\rho_{22}^{(0)}/d_2)$, $K_1 = 1/c+\kappa(p^2\rho_{11}^{(0)}/d_1^2+\rho_{22}^{(0)}/d_2^2)$, and $K_2 = 2\kappa(p^2\rho_{11}^{(0)}/d_1^3+\rho_{22}^{(0)}/d_2^3)$.

Equation (10) consists of two simple Lorentzian terms, corresponding to the resonances between $|3\rangle$ and $|1\rangle$ and between $|3\rangle$ and $|2\rangle$, respectively. Thus only an AT splitting in the absorption spectrum of the probe field occurs. This tells us in the Λ-type system the SGC has no effect on the linear dispersion and absorption spectra of the system. Shown in Shown in Fig. 4(a) and Fig. 4(b) are $\mathrm{Re}(K)$ and $\mathrm{Im}(K)$ as functions of ω. We see that a dip appears in $\mathrm{Im}(K)$ (panel (b)) and, at the same time, the dispersion changes rapidly in

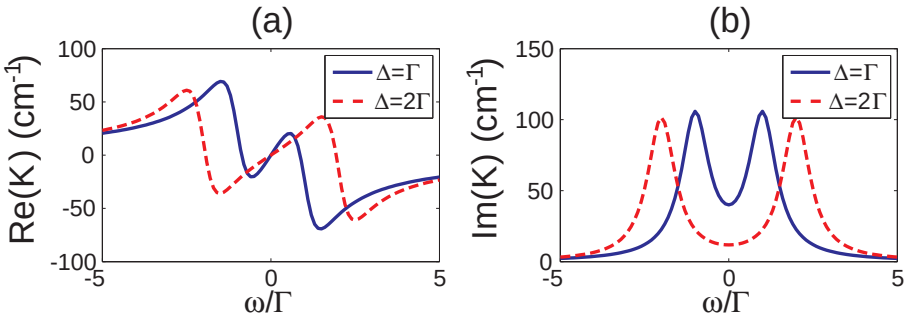

FIG. 4: (color online) Re(K) (panel (a)) and Im(K) (panel (b)) as functions of ω/Γ with $\Delta = \Gamma$ (solid line) and $\Delta = 2\Gamma$ (dashed line).

the region around $\omega = 0$ ((panel (a)). In addition, Re(K) and Im(K) can be adjusted by changing the value of Δ. The solid (dashed) line in the figure is for $\Delta = \Gamma$ ($\Delta = 2\Gamma$). We see that although Im(K) can be lowered by increasing Δ, it has always a large value. Thus in the present Λ-type system one can not acquire a small absorption for the probe field. We must also point out that the value of Δ can not be adjusted to be too large. This is because for a large Δ the SGC effect disappears.

C. Ξ-type system

We finally consider a three-level Ξ-type system, as shown in Fig. 1(c), in which a weak probe field couples the ground state $|1\rangle$ to the intermediate state $|2\rangle$ and simultaneously couples the state $|2\rangle$ to the excited state $|3\rangle$, as suggested in Ref. [33]. States $|2\rangle$ and $|3\rangle$ decay to $|1\rangle$ and $|2\rangle$ with decay rates Γ_1 and Γ_2, respectively. The MB equations governing the evolution of the atoms and the electric field are given by

$$\dot{\rho}_{11} = \Gamma_2\rho_{22} + i\Omega_p^*\rho_{21} - i\Omega_p\rho_{12}, \tag{11a}$$

$$\dot{\rho}_{33} = -\Gamma_3\rho_{33} + ip\Omega_p\rho_{23} - ip\Omega_p^*\rho_{32}, \tag{11b}$$

$$\dot{\rho}_{21} = \left(-i\delta - \frac{\Gamma_2}{2}\right)\rho_{21} + i\Omega_p(\rho_{11} - \rho_{22}) + ip\Omega_p^*\rho_{31} + \eta\sqrt{\Gamma_2\Gamma_3}\rho_{32}, \tag{11c}$$

$$\dot{\rho}_{31} = \left[-i2\left(\Delta + \delta\right) - \frac{\Gamma_3}{2}\right]\rho_{31} + ip\Omega_p\rho_{21} - i\Omega_p\rho_{32}, \tag{11d}$$

$$\dot{\rho}_{32} = \left[-i(2\Delta + \delta) - \frac{\Gamma_2 + \Gamma_3}{2}\right]\rho_{32} + ip\Omega_p(\rho_{22} - \rho_{33}) - i\Omega_p^*\rho_{31}, \tag{11e}$$

$$i\left(\frac{\partial}{\partial z} + \frac{1}{c}\frac{\partial}{\partial t}\right)\Omega_p + \kappa(\rho_{21} + p\rho_{32}) = 0, \tag{11f}$$

with $\rho_{11}+\rho_{22}+\rho_{33}=1$, where $\Omega_p=|\mathbf{e}_p\cdot\mathbf{d}_{12}|\mathcal{E}_p/\hbar$ is half Rabi frequency of the probe field, $\Delta=(E_3-2E_2+E_1)/(2\hbar)$ is half frequency difference of the transitions $|1\rangle\leftrightarrow|2\rangle$ and $|2\rangle\leftrightarrow|3\rangle$, and $\delta=(E_2-E_1)/\hbar-\omega_p$ is one-photon detuning [see Fig. 1(c)]. The last term on the RHS of Eq. (11c) comes from the SGC effect, with $\eta=\mathbf{d}_{12}\cdot\mathbf{d}_{23}/|\mathbf{d}_{12}||\mathbf{d}_{23}|=\cos\theta$. In Eq. (11), $p=|\mathbf{e}_p\cdot\mathbf{d}_{23}|/|\mathbf{e}_p\cdot\mathbf{d}_{12}|$.

Using the MB Eq. (11) we obtain the linear dispersion relation of the system

$$K(\omega)=\frac{\omega}{c}-\kappa\frac{1}{\omega-\delta+i\Gamma_2/2}. \tag{12}$$

From this formula, we see that: (i) The SGC in the Ξ-type system also does not change the linear dispersion and absorption spectra of the probe field; (ii) No dip structure in the absorption spectrum is observed because the system does not possess any AT splitting. Because the peak of the absorption spectrum locates at the center frequency of the probe pulse, a long-distance wave propagation of the probe pulse is not possible in the system. This is not interesting for wave-propagation problem and hence we discard this model in the following discussion.

III. PULSE PROPAGATION IN NONLINEAR REGIME

A. V-type system

Kerr nonlinearity is essential for most nonlinear optical processes. It can be largely enhanced in resonant optical media, but usually a serious optical absorption is also accompanied simultaneously. However, here we show that by the joint action of the AT splitting and the SGC effect, the Kerr nonlinearity in the V-type system can be enhanced greatly with the optical absorption eliminated greatly.

The probe-field susceptibility for the V-type system is defined as

$$\chi_p=\frac{\mathcal{N}_a|\mathbf{e}_p\cdot\mathbf{d}_{12}|^2}{\epsilon_0\hbar}\frac{\rho_{21}+p\rho_{31}}{\Omega_p}\simeq\chi_p^{(1)}+\chi_p^{(3)}|\mathcal{E}_p|^2, \tag{13}$$

where $\chi_p^{(1)}$ and $\chi_p^{(3)}$ are linear and third-order susceptibilities, respectively. The real part of $\chi_p^{(3)}$ contributes to the Kerr nonlinearity while the imaginary part of $\chi_p^{(3)}$ contributes to the nonlinear absorption or gain of the system. The explicit expressions of $\chi_p^{(1)}$ and $\chi_p^{(3)}$ can be

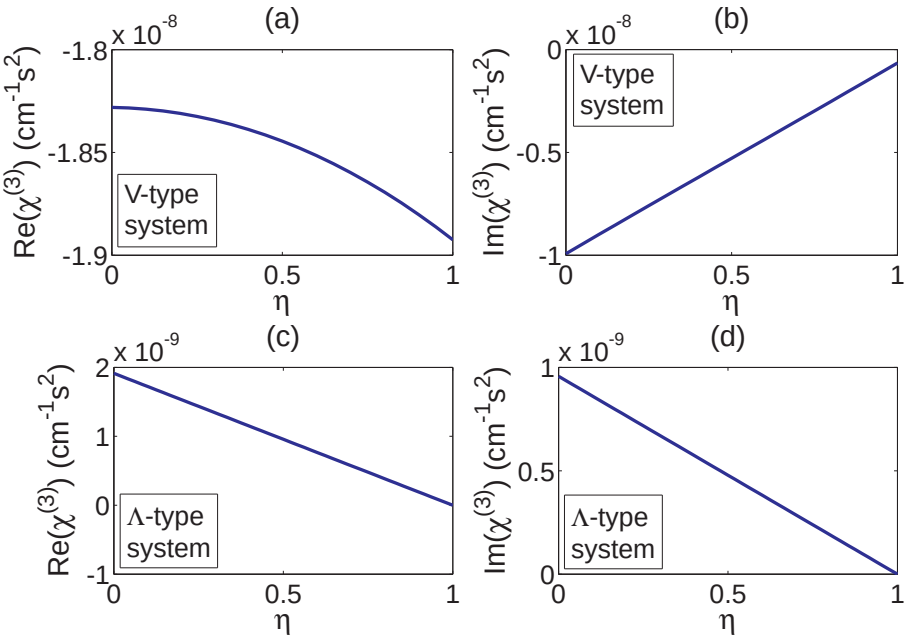

FIG. 5: (color online) (a) and (b): $\mathrm{Re}(\chi^{(3)})$ and $\mathrm{Im}(\chi^{(3)})$ as functions of η for the V-type system, respectively. (c) and (d): $\mathrm{Re}(\chi^{(3)})$ and $\mathrm{Im}(\chi^{(3)})$ as functions of η for the Λ-type system, respectively.

obtained by solving Eq. (2) under steady-state approximation, which reads

$$\chi_p^{(1)} = -\frac{\mathcal{N}_a|\mathbf{e}_p\cdot\mathbf{d}_{12}|^2}{\epsilon_0\hbar}\frac{p^2d_2+d_3-ip\eta\Gamma}{d_2d_3+\eta^2\Gamma^2/4}, \tag{14a}$$

$$\chi_p^{(3)} = \frac{\mathcal{N}_a|\mathbf{e}_p\cdot\mathbf{d}_{12}|^4}{\epsilon_0\hbar^3}\frac{d_2A+d_3B-i\eta\Gamma C/2}{d_2d_3+\eta^2\Gamma^2/4}, \tag{14b}$$

with the explicit expressions of A, B, and C being given in Appendix A. Shown in Fig. 5(a) and Fig. 5(b) are $\mathrm{Re}(\chi^{(3)})$ and $\mathrm{Im}(\chi^{(3)})$ as functions of η, respectively. System parameters are taken as $\mathcal{N}_a = 10^7$ cm^{-3}, $d_{13}\approx d_{23} = 2.5\times10^{-27}$ cm C, $\Gamma = 1.0\times10^7$ s^{-1}, $\Delta = 5.5\times10^7$ s^{-1}, $\delta = 1.0\times10^7$ s^{-1}, and $p = 1$. From the figure we see that $|\mathrm{Re}(\chi^{(3)})|$ grows as η increases, whereas $|\mathrm{Im}(\chi^{(3)})|$ is reduced as η increases. The condition $|\mathrm{Re}(\chi^{(3)})| \gg |\mathrm{Im}(\chi^{(3)})|$ holds in the whole range of η. Thus, the SGC effect enhances the Kerr nonlinearity of the system significantly. In addition, $\mathrm{Re}(\chi^{(3)})$ has an order of 10^{-8} cm^{-1} s^2, i.e. it is 10^{12} times larger than that of conventional nonlinear optical media [34].

The Kerr nonlinearity enhancement obtained above can be used to balance the dispersion of the system and hence to obtain a lossless and distortionless optical pulse propagation in nonlinear regime. To this end we apply the standard multiple-scale method [9], which is beyond the steady-state and adiabatic approximations, to solve Eqs. (2) and (3). We make

the following asymptotic expansion $\rho_{jj} = \delta_{1j} + \sum_{n=1}^{\infty} \epsilon^n \rho_{jj}^{(n)}$ ($j = 1, 2, 3$), $\rho_{ij} = \sum_{n=1}^{\infty} \epsilon^n \rho_{ij}^{(n)}$ ($i, j = 1, 2, 3$; $i \neq j$), and $\Omega_p = \sum_{n=1}^{\infty} \epsilon^n \Omega_p^{(n)}$, where ϵ is a small parameter characterizing the small population depletion of the ground state. To obtain a divergence-free expansion, all quantities on the right hand side of the expansion are considered as functions of the multi-scale variables $z_l = \epsilon^l z$ ($l = 0, 1, 2$) and $t_l = \epsilon^l t$ ($l = 0, 1$). Substituting the expansion and the multi-scale variables into Eqs. (2) and (3), we obtain a chain of linear, but inhomogeneous equations which can be solved order by order.

At the leading order, we get the linear solution $\Omega_p^{(1)} = F \exp\{i[K(\omega)z_0 - \omega t_0]\}$ and the dispersion relation, given by Eq. (4). At the second order, a divergence-free condition requires $\partial F/\partial z_1 + (1/V_g)\partial F/\partial t_1 = 0$. Here F is a yet to be determined envelope function depending on the slow variables t_1, z_1 and z_2. At the third order, we obtain the nonlinear equation for F:

$$i\frac{\partial F}{\partial z_2} - \frac{K_2}{2}\frac{\partial^2 F}{\partial t_1^2} - W \exp(-\bar{\beta} z_2)\, F|F|^2 = 0, \tag{15}$$

where $\bar{\beta} = \epsilon^{-2}\beta$ with $\beta = 2\mathrm{Im}(K_0)$ and

$$W = -\kappa \frac{d_2 A + d_3 B - i\eta\Gamma C/2}{d_2 d_3 + \eta^2 \Gamma^2/4}. \tag{16}$$

After returning to original variables, Eq. (15) becomes

$$i\left(\frac{\partial}{\partial z} + \frac{\beta}{2}\right) U - \frac{K_2}{2}\frac{\partial^2 U}{\partial \tau^2} - W|U|^2 U = 0, \tag{17}$$

where $\tau = t - z/V_g$ and $U = \epsilon F e^{-\bar{\beta} z_2/2}$. Equation (17) usually has complex coefficients due to the resonant character of the system. However, as we shall show below, under the joint action of the SGC and the AT splitting, practical set of system parameters can be found to make the imaginary part of the coefficients be much smaller than their real part. Then Eq. (17) can be approximated as a nonlinear Schrödinger (NLS) equation, which allows soliton solutions being able to propagate for a rather long distance without significant attenuation and distortion. The dimensionless form of Eq. (17) is

$$i\frac{\partial u}{\partial s} + \frac{\partial^2 u}{\partial \sigma^2} + 2u|u|^2 = i2\mu u, \tag{18}$$

where $s = -z/(2L_D)$, $\sigma = \tau/\tau_0$, and $u = U/U_0$, $\mu = L_D/L_A$, with $L_D = \tau_0^2/|\tilde{K}_2|$ being the characteristic dispersion length, $L_A = 1/\beta$ the characteristic absorption length, and $U_0 = (1/\tau_0)\sqrt{|\tilde{K}_2/\tilde{W}|}$ the characteristic Rabi frequency of the probe field. The symbol tilde denotes the real part of the corresponding quantity.

If L_D is much less than L_A (i.e., $\mu \ll 1$, which is the case in the presence of the SGC), the term on the right-hand side of Eq. (18) can be treated as a small perturbation and can be neglected at the first order. Hence Eq. (18) reduces to the standard NLS equation, which is completely integrable and allows multi-soliton solutions. After returning to the original variables, a single soliton solution of the NLS equation corresponds to

$$\Omega_p = \frac{1}{\tau_0}\sqrt{\frac{\tilde{K}_2}{\tilde{W}}}\,\mathrm{sech}\left[\frac{1}{\tau_0}\left(t-\frac{z}{\tilde{V}_g}\right)\right]\exp\left[i\phi z - i\frac{z}{2L_D}\right]. \tag{19}$$

We now present a practical numerical example to support the above results. Consider a cold alkali atomic gas, for which the system parameters can be taken as $d_{24} \approx d_{34} = 2.5 \times 10^{-27}$ cm C, $\kappa = 1.0\times10^9$ cm^{-1} s^{-1}, $\Gamma_2 \approx \Gamma_3 = 1.0\times10^7$ s^{-1}, $\Delta = 5.5\times10^7$ s^{-1}, $\delta = 1.0\times10^7$ s^{-1}, $\eta = 1$, and $p = 1$. Then we obtain $K_0 = 6.83 + i0.23$ cm^{-1}, $K_1 = (0.73 - i0.05)\times10^{-6}$ cm^{-1}s, $K_2 = (0.14 + i0.06)\times10^{-13}$ cm^{-1}s^2, and $W = (1.00 + i0.03)\times10^{-14}$ cm^{-1}s^2. Notice that the imaginary parts of these quantities are indeed much smaller than their real parts. The reason is that the SGC plays an important role to make the optical absorption of the system be largely eliminated. Taking $\tau_0 = 0.8\times10^{-7}$ s, we have $L_D = 0.45$ cm, $U_0 = 1.5\times10^7$ s^{-1}, and $L_A = 4.3$ cm ($\mu \approx 0.1$). Then the propagating velocity of the soliton is given by

$$\tilde{V}_g = 4.6\times10^{-5}\,c, \tag{20}$$

i.e., the soliton formed in the V-type system travels indeed with an ultraslow velocity. We must stress that the present scheme for generating the ultraslow optical soliton needs only one laser field, which is different from the EIT scheme, where at least two laser fields are required [9–12].

With the above parameters, it is easy to estimate the peak power of the ultraslow optical soliton by using the Poyntings vector, which reads

$$\bar{P}_{\mathrm{peak}} = 0.65\,\mu W, \tag{21}$$

where the cross-section area of the probe laser beam is taken to be $\pi\times10^{-4}$ cm^2. Thus, we see that very low input power is needed for generating the ultraslow optical soliton due to the enhancement of Kerr nonlinearity.

We have also studied the stability of the ultraslow optical soliton presented above by using numerical simulations. Shown in Fig. 6(a) is the wave shape of $|\Omega_p/U_0|^2$ as a function

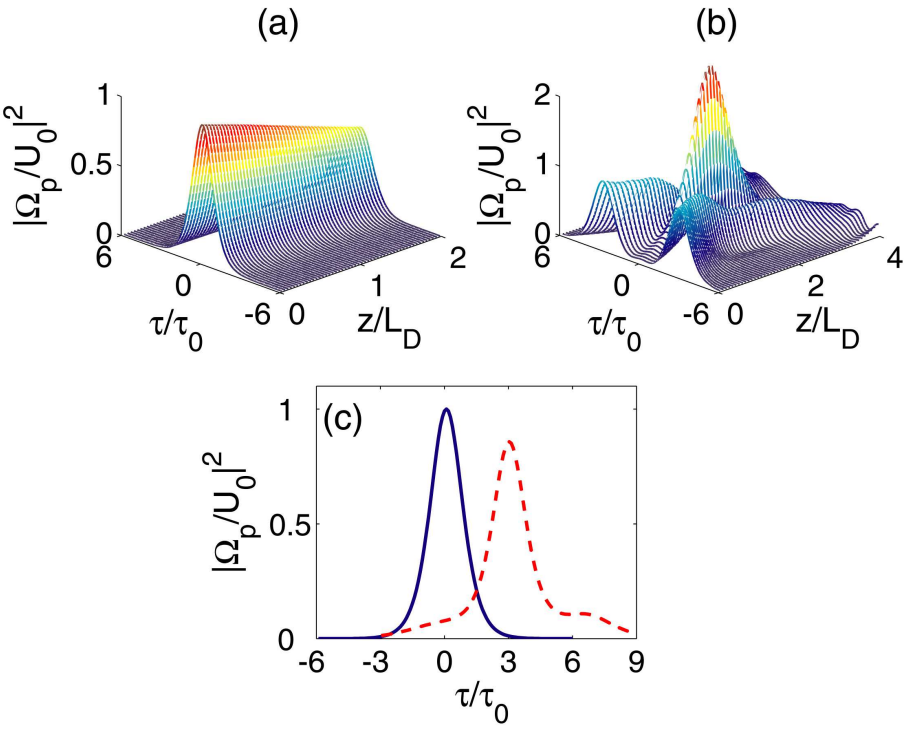

FIG. 6: (color online) (a): Waveshape of $|\Omega_p/U_0|^2$ as a function of z/L_D and τ/τ_0. The solution is numerically obtained from Eq. (17) with full complex coefficients taken into account. (b): Collision between two ultraslow solitons. (c): Waveshape of $|\Omega_p/U_0|^2$ as a function of τ/τ_0 by directly integrating Eqs. (2) and (3) at $z = 0$ (solid line) and $z = 2L_D$ (dashed line).

of z/L_D and τ/τ_0 based on Eq. (17). We see that the amplitude of the soliton undergoes only a slight decrease and its width undergoes a slight increase after propagating to a long distance. A simulation of the interaction between two ultraslow optical solitons is also carried out by initially inputting two identical solitons [see Fig. 6(b)]. As time goes on, the two solitons collide, pass through, and depart from each other. They recover basically their initial waveforms after the collision. Finally, we have also made a numerical simulation by directly integrating Eqs. (2) and (3) to confirm the analytical prediction, with the result shown in Fig. 6(c).

B. Λ-type system

The probe-field susceptibility for the Λ-type system is

$$\chi_p = \frac{\mathcal{N}_a|\mathbf{e}_p\cdot\mathbf{d}_{12}|^2}{\epsilon_0\hbar}\frac{p\rho_{31}+\rho_{32}}{\Omega_p} \simeq \chi_p^{(1)} + \chi_p^{(3)}|\mathcal{E}_p|^2, \tag{22}$$

where

$$\begin{aligned}
\chi_p^{(1)} &= \frac{\mathcal{N}_a|\mathbf{e}_p\cdot\mathbf{d}_{12}|^2}{\epsilon_0\hbar}\left(p^2\frac{\rho_{11}^{(0)}}{d_1}+\frac{\rho_{22}^{(0)}}{d_2}\right),\\
\chi_p^{(3)} &= \frac{\mathcal{N}_a|\mathbf{e}_p\cdot\mathbf{d}_{12}|^4}{\epsilon_0\hbar^3}\left(\frac{-A+B+C}{d_1}+\frac{-2A+B^*-C}{d_2}\right),
\end{aligned} \tag{23}$$

with $A = ip\rho_{11}^{(0)}(1/d_1^*-1/d_1)/\Gamma$, $B = (p\rho_{11}^{(0)}/d_1 - p\rho_{22}^{(0)}/d_2^* - i\eta\Gamma A/2)/(2\Delta)$, and $C = [X_1A - p|d_1|^2(d_2B - d_2^*B^*) - |d_2|^2(d_1^*B - d_1B^*)]/X_2$ with $X_1 = -i\Gamma(2|d_1|^2 - p|d_2|^2)$, and $X_2 = i\Gamma(|d_1|^2 + p|d_2|^2)$.

Shown in Fig. 5(c) and Fig. 5(d) are $\mathrm{Re}(\chi^{(3)})$ and $\mathrm{Im}(\chi^{(3)})$ as functions of the SGC parameter η. The values of the system parameters are the same with those used for the V-type system. We see that both $\mathrm{Re}(\chi^{(3)})$ and $\mathrm{Im}(\chi^{(3)})$ decreases rapidly as η grows, i.e., the SGC effect weakens the Kerr nonlinearity of the system. Based on this reason and on the large linear optical absorption shown in the last section, we conclude that an ultraslow optical soliton is not possible in the present Λ-type system.

IV. THE CASE FOR OPEN SYSTEMS

The results presented above are valid only for close systems. However, realistic physical systems, in particular molecules [35], are usually open ones in which additional spontaneous decay pathways from upper levels to some other lower levels exist and hence spoil quantum coherence. In this section, we examine an open system related to V-type configuration and show that the additional decay pathways may lead to different initial population distribution of the states $|1\rangle$, $|2\rangle$, and $|3\rangle$ and hence are detrimental to the SGC of the system.

Consider an extended V-type system with its main part the same as Fig. 1(a), but the two closely spaced upper levels $|2\rangle$ and $|3\rangle$ may decay into the fourth state $|4\rangle$ with spontaneous decay rates Γ_2' and Γ_3', respectively. In addition, a transient relaxation rate γ is introduced to denote the leaving and entering of particles in light-particle interaction region; see Fig. 7. Notice that in this simplified description the state $|4\rangle$ represents many other ground-state

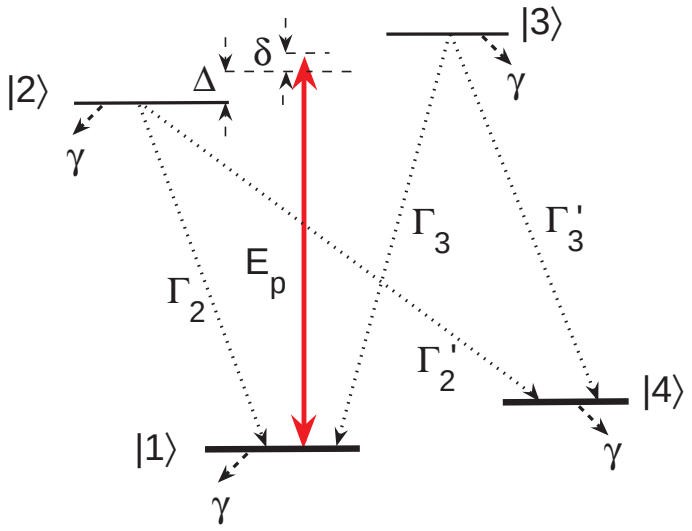

FIG. 7: (color online) Model scheme of the open system related to V-type level configuration. Two closely spaced upper levels, $|2\rangle$ and $|3\rangle$, decay into the fourth state $|4\rangle$ with spontaneous decay rates Γ_2' and Γ_3', respectively. $|j\rangle$ $(j = 1, 2, 3, 4)$ are bare states, $\mathbf{E}_p$ is the probe laser field, Δ and δ are detunings. γ is the transient relaxation rate of the particles leaving and entering light-particle interaction region.

sublevels that provide various relaxation pathways from the two upper sates $|2\rangle$ and $|3\rangle$. The equations of motion for the density matrix of the system are

$$\dot{\rho}_{11} = -\gamma(\rho_{11} - \rho_{11}^{\rm eq}) + \Gamma_2\rho_{22} + \Gamma_3\rho_{33} - i\Omega_p\rho_{12} + i\Omega_p^*\rho_{21} - ip\Omega_p\rho_{13} + ip\Omega_p^*\rho_{31} + \eta\sqrt{\Gamma_2\Gamma_3}(\rho_{23} + \rho_{32}), \tag{24a}$$

$$\dot{\rho}_{22} = -\gamma(\rho_{22} - \rho_{22}^{\rm eq}) - (\Gamma_2 + \Gamma_2')\rho_{22} + i\Omega_p\rho_{12} - i\Omega_p^*\rho_{21} - \eta\frac{\sqrt{\Gamma_2\Gamma_3}}{2}(\rho_{23} + \rho_{32}), \tag{24b}$$

$$\dot{\rho}_{33} = -\gamma(\rho_{33} - \rho_{33}^{\rm eq}) - (\Gamma_3 + \Gamma_3')\rho_{33} + ip\Omega_p\rho_{13} - ip\Omega_p^*\rho_{31} - \eta\frac{\sqrt{\Gamma_2\Gamma_3}}{2}(\rho_{23} + \rho_{32}), \tag{24c}$$

$$\dot{\rho}_{44} = -\gamma(\rho_{44} - \rho_{44}^{\rm eq}) + \Gamma_2'\rho_{22} + \Gamma_3'\rho_{33}, \tag{24d}$$

$$\dot{\rho}_{21} = \left[i(\Delta + \delta) - \frac{\Gamma_2 + \Gamma_2'}{2}\right]\rho_{21} + i\Omega_p(\rho_{11} - \rho_{22}) - ip\Omega_p\rho_{23} - \eta\frac{\sqrt{\Gamma_2\Gamma_3}}{2}\rho_{31}, \tag{24e}$$

$$\dot{\rho}_{31} = \left[i(-\Delta + \delta) - \frac{\Gamma_3 + \Gamma_3'}{2}\right]\rho_{31} + ip\Omega_p(\rho_{11} - \rho_{33}) - i\Omega_p\rho_{32} - \eta\frac{\sqrt{\Gamma_2\Gamma_3}}{2}\rho_{21}, \tag{24f}$$

$$\dot{\rho}_{32} = -\left(i2\Delta + \frac{\Gamma_2 + \Gamma_2' + \Gamma_3 + \Gamma_3'}{2}\right)\rho_{32} - i\Omega_p^*\rho_{31} + ip\Omega_p\rho_{12} - \eta\frac{\sqrt{\Gamma_2\Gamma_3}}{2}(\rho_{22} + \rho_{33}), \tag{24g}$$

with $\rho_{4j} = 0$ $(j = 1, 2, 3)$. Here $\rho_{jj}^{\rm eq}$ $(j = 1, 2, 3, 4)$ is the population of thermal equilibrium

when the light field and the spontaneous emission are absent. The equation of motion for the probe-field Rabi frequency Ω_p is still given by Eq. (3). Note that $\sum_{j=1}^{3}\rho_{jj}\neq 1$ is broken for the present system.

When the probe field is absent, the steady-state solution of the system reads

$$\rho_{11}=\frac{\Gamma(\rho_{22}+\rho_{33})+\eta\Gamma(\rho_{32}+\rho_{23})}{\gamma}+\rho_{11}^{\rm eq}, \tag{25a}$$

$$\rho_{22}=\frac{M_1\rho_{22}^{eq}+M_2\rho_{33}^{\rm eq}}{M}, \tag{25b}$$

$$\rho_{33}=\frac{M_1\rho_{33}^{eq}+M_2\rho_{22}^{\rm eq}}{M}, \tag{25c}$$

$$\rho_{32}=\frac{(\gamma+\Gamma+\Gamma')(2i\Delta-\Gamma-\Gamma')\eta\Gamma/2}{M}\gamma(\rho_{22}^{eq}+\rho_{33}^{\rm eq}), \tag{25d}$$

$$\rho_{44}=\frac{\Gamma'(\rho_{22}+\rho_{33})}{\gamma}+\rho_{44}^{\rm eq}, \tag{25e}$$

with other $\rho_{jl}=0$, where $M_1=4\gamma(\gamma+\Gamma+\Gamma')\Delta^2+\gamma(\Gamma+\Gamma')[(\Gamma+\Gamma')^2+\gamma(\Gamma+\Gamma')-\eta^2\Gamma^2/2]$, $M_2=\gamma(\Gamma+\Gamma')\eta^2\Gamma^2/2$, and $M=-(\Gamma+\Gamma')(\gamma+\Gamma+\Gamma')\eta^2\Gamma^2+(\gamma+\Gamma+\Gamma')^2[(\Gamma+\Gamma')^2+4\Delta^2]$. For simplicity we have assumed $\Gamma_2\approx\Gamma_3=\Gamma$ and $\Gamma_2'\approx\Gamma_3'=\Gamma'$. One sees that there are non-zero initial population in the states $|2\rangle$, $|3\rangle$, and $|4\rangle$ due to non-zero Γ_2', Γ_3', and $\rho_{jj}^{\rm eq}$.

It is easy to obtain the linear dispersion relation of the system

$$\begin{aligned}K(\omega) \;=\; & \frac{\omega}{c}-\kappa\left[\frac{(\omega+g_3)(\rho_{11}-\rho_{22})-ip\eta\Gamma(\rho_{11}-\rho_{33})/2}{D(\omega)}\right.\\ & \left.+\frac{p^2(\omega+g_2)(\rho_{11}-\rho_{33})-ip\eta\Gamma(\rho_{11}-\rho_{22})/2}{D(\omega)}\right],\end{aligned} \tag{26}$$

where $D(\omega)=(\omega+d_2)(\omega+d_3)+\eta^2\Gamma^2/4$ with $d_2=\Delta+\delta+i(\Gamma+\Gamma')/2$ and $d_3=-\Delta+\delta+i(\Gamma+\Gamma')/2$. Illustrated in Fig. 8(a) and Fig. 8(b) are respectively the spectra of $\mathrm{Re}(K)$ and $\mathrm{Im}(K)$ as functions of ω for $\Gamma'=0.01\Gamma$ (the dashed line), $\Gamma'=0.1\Gamma$ (the solid line), and $\Gamma'=\Gamma$ (the dash-dotted line). When plotting the figure, the value of γ is chosen to be $10^{-2}\Gamma$ [36]. In addition, η is taken to unity in order to show clearly the influence of the decay rates Γ_2' and Γ_3' with the maximum SGC. From Eq. (26) and Fig. 8 we obtain the following conclusions: (i) Due to the open character of the system (i.e. the existence of the additional spontaneous decay pathways from the states $|2\rangle$, $|3\rangle$ to the state $|4\rangle$), the slope of $\mathrm{Re}(K)$ curve with respect to ω decreases when Γ' increases, which means that the group velocity of the probe field becomes larger when Γ' grows; see Fig 8(a). (ii) The absorption of the probe field can not be completely eliminated by means of the SGC effect, i.e. the system is always absorptive. In particular, the minimum of the absorption spectrum increases when

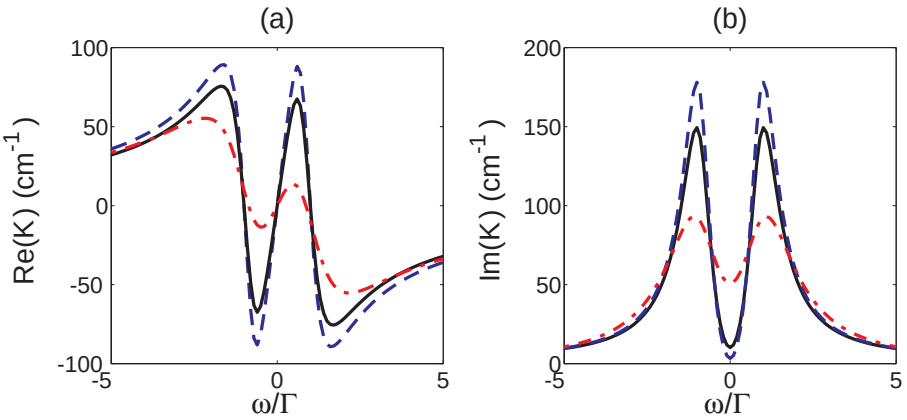

FIG. 8: (color online) Re(K) (panel (a)) and Im(K) (panel (b)) as functions of ω/Γ for $\Gamma' = 0.01\Gamma$ (dashed line), $\Gamma' = 0.1\Gamma$ (solid line), and $\Gamma' = \Gamma$ (dash-dotted line).

Γ' increases; see Fig 8(b). This tells us that the additional spontaneous decay pathways in the open system are detrimental to the SGC. Such conclusions can also be understood in another way. In order to suppress the absorption of the probe field, it is necessary to keep the most of atoms populated in the ground state $|1\rangle$. Nevertheless, from Eq. (25) we see that the additional spontaneous decay pathways distribute the population of the ground state into other ground-state sublevels. In addition, when Γ' grows, the population in the state $|4\rangle$ also grows, which results in the destruction of the quantum coherence of the system. Consequently, a quantum coherence with zero (linear) absorption based on the SGC takes place only in closed systems. However, as shown in Fig. 8(b), although in an open system a high-quality quantum coherence can not be realized, a significant suppression of probe-field absorption can still occur, as shown by the recent experimental observation in a molecular system [35].

V. DISCUSSION AND SUMMARY

Notice that the SGC occurs in systems having near-degenerated levels with the same angular momentum quantum numbers J and m_J and nonorthogonal dipole moments, which are rarely satisfied for realistic atomic systems [37]. However, such type of quantum interference can be observed in many other systems such as semiconductor quantum wells and quantum dots [38–40], autoionizing media [41], and anisotropic vacuum [42]. Our theoretical approach presented above can be easily generalized to these systems with the SGC.

In summary, in this work we have investigated the linear and nonlinear pulse propagations in lifetime-broadened three-state media with SGC. Three generic systems of V-, Λ-, and Ξ-type level configurations have been considered and compared. We have shown that in the linear propagation regime the SGC in the V-type system can result in a significant change of dispersion and absorption and may be used to completely eliminate the absorption and largely reduce the group velocity of the probe field. However, the SGC has no effect on the dispersion and absorption of the Λ- and Ξ-type systems. We have also shown that in the nonlinear propagation regime, the SGC displays different influences on Kerr nonlinearity for different systems. In particular, it can enhance the Kerr nonlinearity of the V-type system whereas weaken the Kerr nonlinearity of the Λ-type system. By exploiting the SGC effect, stable optical solitons with ultraslow propagating velocity and very low pump power can be produced in the V-type system by using only a single laser field in the system.

Acknowledgments

This work was supported by the National Natural Science Foundation of China under Grant No. 10874043, and by the Open Fund from the State Key Laboratory of Precision Spectroscopy, ECNU.

Appendix A: The expressions of A, B, and C in $\chi_p^{(3)}$

The expressions of A, B, and C in $\chi_p^{(3)}$ and W are given as $A = pX_1 + 2pX_2 + X_3^*$, $B = 2X_1 + X_2 + pX_3$, and $C = (2+p)X_1 + (2p+1)X_2 + pX_3 + X_3^* = A + B$, where

$$\begin{aligned} X_1 &= \frac{2(Y_1 - Y_2)\zeta^2 + [\Gamma(Y_3 + Y_4) + i2\Delta(Y_3 - Y_4)]\zeta - (\Gamma^2 + 4\Delta^2)Y_1}{\Gamma(\Gamma^2 + 4\Delta^2 - 4\zeta^2)}, \\ X_2 &= \frac{2(Y_2 - Y_1)\zeta^2 + [\Gamma(Y_3 + Y_4) + i2\Delta(Y_3 - Y_4)]\zeta - (\Gamma^2 + 4\Delta^2)Y_2}{\Gamma(\Gamma^2 + 4\Delta^2 - 4\zeta^2)}, \\ X_3 &= \frac{2(Y_3 - Y_4)\zeta^2 + [(\Gamma + i2\Delta)(Y_1 + Y_2)]\zeta - \Gamma(\Gamma + 2i\Delta)Y_3}{\Gamma(\Gamma^2 + 4\Delta^2 - 4\zeta^2)}, \end{aligned} \tag{A1}$$

with

$$
\begin{aligned}
Y_1 &= -\frac{d_3 - ip\zeta}{d_2 d_3 + \zeta^2} + \frac{d_3^* + ip\zeta}{d_2^* d_3^* + \zeta^2}, \\
Y_2 &= -\frac{p^2 d_2 - ip\zeta}{d_2 d_3 + \zeta^2} + \frac{p^2 d_2^* + ip\zeta}{d_2^* d_3^* + \zeta^2}, \\
Y_3 &= -\frac{d_3 - ip\zeta}{d_2 d_3 + \zeta^2} + \frac{p^2 d_2^* + ip\zeta}{d_2^* d_3^* + \zeta^2}, \\
Y_4 &= -\frac{p^2 d_2 - ip\zeta}{d_2 d_3 + \zeta^2} + \frac{d_3^* + ip\zeta}{d_2^* d_3^* + \zeta^2},
\end{aligned}
\tag{A2}
$$

and $\zeta = \eta\Gamma/2$.

---

[1] M. J. Konopnicki and J. H. Eberly, Phys. Rev. A 24, 2567 (1981); R. Grobe, F. T. Hioe, and J. H. Eberly, Phys. Rev. Lett. **73**, 3183 (1994).

[2] L. V. Hau, S. E. Harris, Z. Dutton, and C. H. Behroozi, Nature (London) **397**, 594 (1999).

[3] C. Liu, Z. Dutton, C. H. Behroozi, and L. V. Hau, Nature (London) **409**, 490 (2001).

[4] D. F. Phillips, A. Fleischhauer, A. Mair, R. L. Walsworth, and M. D. Lukin, Phys. Rev. Lett. **86**, 783 (2001).

[5] M. D. Eisaman, A. André, F. Massou, M. Fleischhauer, A. S. Zibrov, and M. D. Lukin, Nature (London) **438**, 837 (2005).

[6] M. Fleischhauer, A. Imamoglu and J. P. Marangos, Rev. Mod. Phys. **77**, 633 (2005), and references therein.

[7] M. D. Lukin, P.R. Hemmer, M. Löfler, and M. O. Scull, **81**, 2675 (1998).

[8] L. Deng, M. Kozuma, E. W. Hagley, and M. G. Payne, Phys. Rev. Lett. **88**, 143902 (2002).

[9] Y. Wu and L. Deng, Phys. Rev. Lett. **93**, 143904 (2004); G. Huang, L. Deng, and M. G. Payne, Phys. Rev. E **72**, 016617 (2005); C. Hang, G. Huang, and L. Deng, Phys. Rev. E **73**, 036607 (2006).

[10] H. Michinel and M. J. Paz-Alonso, and V. M. Pérez-García, Phys. Rev. Lett. **96**, 023903 (2006).

[11] C. Hang, G. Huang, and L. Deng, Phys. Rev. E **73**, 046601 (2006); C. Hang, V. V. Konotop, and G. Huang, Phys. Rev. A **79**, 033826 (2009); C. Hang and V. V. Konotop, Phys. Rev. A **83**, 053845 (2011).

[12] Y. Zhang, Z. Wang, H. Zheng, C. Yuan, C. Li, K. Lu, and M. Xiao, Phys. Rev. A **82**, 053837 (2010); Y. Zhang, Z. Wang, Z. Nie, C. Li, H. Chen, K. Lu, and M. Xiao, Phys. Rev. Lett. **106**, 093904 (2011).

[13] A. K. Mohapatra, T. R. Jackson, and C. S. Adams, Phys. Rev. Lett. **98**, 113003 (2007); K. J. Weatherill, J. D. Pritchard, R. P. Abel, M. G. Bason, A. K. Mohapatra and C. S. Adams, J. Phys. B: At. Mol. Opt. Phys., **41**, 201002 (2008).

[14] S. E. Harris, Phys. Rev. Lett. **62**, 1033 (1989); A. Imamoğlu, Phys. Rev. A **40**, 2835 (1989).

[15] J. H. Wu and J. Y. Gao, Phys. Rev. A **65**, 063807 (2002).

[16] Y. Bai, H. Guo, H. Sun, D. Han, C. Liu, and X. Chen, Phys. Rev. A **69**, 043814 (2004).

[17] S. Menon and G. S. Agarwal, Phys. Rev. A **57**, 4014 (1998).

[18] S. Y. Zhu, R. C. F. Chan, and C. P. Lee, Phys. Rev. A **52**, 710 (1995); S. Y. Zhu and M. O. Scully, Phys. Rev. Lett. **76**, 388 (1996).

[19] P. Zhou and S. Swain, Phys. Rev. Lett. **77**, 3995 (1996).

[20] E. Paspalakis and P. L. Knight, Phys. Rev. Lett. **81**, 293 (1998).

[21] K. T. Kapale, M. O. Scully, S. Y. Zhu, and M. S. Zubairy, Phys. Rev. A **67**, 023804 (2003).

[22] I. Gonzalo, M. A. Antón, F. Carreño, and O. G. Calderón, Phys. Rev. A **72**, 033809 (2005).

[23] Y. P. Niu and S. Q. Gong, Phys. Rev. A **73**, 053811 (2006).

[24] D. G. Norris, L. A. Orozco, P. Barberis-Blostein, and H. J. Carmichael, Phys. Rev. Lett. **105**, 123602 (2010).

[25] Z. Tang, G. Li, and Z. Ficek, Phys. Rev. A **82**, 063837 (2010).

[26] R. G. Wan, J. Kou, L. Jiang, Y. Jiang, and J. Y. Gao, Phys. Rev. A **83**, 033824 (2011).

[27] E. Paspalakis, N. J. Kylstra, and P. L. Knight, Phys. Rev. Lett. **82**, 2079 (1999).

[28] D. A. Cardimona, M. G. Raymer, and C. R. Stroud, Jr., J. Phys. B **15**, 65 (1982).

[29] The frequency and wavenumber of the probe field are given by $\omega_p + \omega$ and $k_p + K(\omega)$, respectively. Thus $\omega = 0$ corresponds to the center frequency of the probe field.

[30] T. Y. Abi-Salloum, Phys. Rev. A **81**, 053836 (2010); P. M. Anisimov, J. P. Dowling, and B. C. Sanders, arXiv: 1102.0546v1.

[31] J. Javanainen, Europhys. Lett. **17**, 407 (1992).

[32] S. Menon and G. S. Agarwal, Phys. Rev. A **57**, 4014 (1998).

[33] Z. Ficek, B. J. Dalton, and P. L. Knight, Phys. Rev. A **51**, 4062 (1995).

[34] S. Saltiel, S. Tanev, and A. D. Boardman, Opt. Lett. **22**, 148 (1997).

[35] A. Lazoudis, T. Kirova, E. H. Ahmed, P. Qi, J. Huennekens, and A. M. Lyyra, Phys. Rev. A **83**, 063419 (2011).

[36] S. Zhu, D. Wang, and J. Gao, Phys. Rev. A **55**, 1339 (1997).

[37] H. R. Xia, C. Y. Ye, and S. Y. Zhu, Phys. Rev. Lett. **77**, 1032 (1996).

[38] J. Faist, F. Capasso, C. Sirtori, K. W. West, and L. N. Pfeiffer, Nature (London) **390**, 589 (1997).

[39] H. Schmidt, K. L. Campman, A. C. Gossard, and A. Imamoğlu, Appl. Phys. Lett. **70**, 3455 (1997).

[40] J. H. Wu, J. Y. Gao, J. H. Xu, L. Silvestri, M. Artoni, G. C. La Rocca, and F. Bassani, Phys. Rev. Lett. **95**, 057401 (2005).

[41] T. Nakajima, Phys. Rev. A **63**, 043804 (2000); T. Nakajima, Opt. Lett. **25**, 847 (2000).

[42] G. S. Agarwal, Phys. Rev. Lett. **84**, 5500 (2000).